Aust. J. Phys., 1992, **45**, 85–97

Atomic Arrangement of the Clean Si(110) 5×1 Surface Derived by Low Energy Scattering Spectroscopy

Y. G. Shen,[A] *D. J. O'Connor and R. J. MacDonald*

Department of Physics, University of Newcastle,
Newcastle, N.S.W. 2308, Australia.
[A] Present address: Surface Science Western,
University of Western Ontario,
London, Ontario N6A 5B7, Canada.

Abstract

The atomic arrangement of the Si(110) 5×1 reconstructed surface has been studied by low energy ion scattering. The experimentally measured incident angle scan data were compared with the results of computer simulations for various structural models. Although detailed quantitative interpretation of the full range of ion scattering data is difficult to achieve, there is clear evidence for a major reconstruction of the surface. A reasonable fit for the adatom model between the experimental results and computer simulation suggests that the clean Si(110) 5×1 surface consists of a mixture of 5×1, 5×4 and 5×5 structures, possibly partially disordered along the [$\bar{1}$10] direction. The different adatom and rest atom sites have been determined by fitting the calculation with the experimental data. However, there is no other existing experimental evidence, at this time, to support the adatom or rest atom height.

1. Introduction

The Si(110) surface has received considerably less interest than the (111) and (100) surfaces, although this surface is not without technological importance. Only a few studies have been made so far and a large number of ordered surface structures on Si(110) have been observed using low energy electron diffraction (LEED). However, the reconstructions reported therein are not clear. For instance, in the first LEED study of this surface Jona (1965) found seven structures: 'initial', 4×5, 2×1, 5×1, 7×1, 9×1, and '×'. An interesting aspect of this surface was later reported by Olshanetsky and Shklyaev (1977), who interpreted some of these reconstructions in terms of order–order phase transitions with increasing temperature. In particular, on heating a 4×5 reconstructed surface a 2×1 LEED pattern was observed above 600°C, which changed to 5×1 at a temperature of 750°C. Recent LEED (Ichinokawa *et al.* 1985) and reflected high energy electron diffraction (RHEED) (Yamamoto *et al.* 1986) observations suggest that a '16×2' superstructure is the only clean surface structure, while most of the known reconstructions are associated with the presence of small Ni (2–7% ML) impurities. On the other hand, it was argued by Olshanetsky *et al.* (1977) that such '16×2' diffraction patterns are produced by facetted planes with the indices (17 15 1), (15 17 $\bar{1}$), (17 15 $\bar{1}$), and (15 17 1) which contain the 2×1 structure.

0004-9506/92/010085$05.00

It has generally been accepted that the clean Si(110) surface undergoes several higher order reconstructions depending critically on heat treatment, sample history, cooling rate and preparation (Jona 1965; Olshanetsky and Shklyaev 1977); the evidence for this was, however, not completely clear. Of several different reconstructions, more attention has been focused on the 5×1 structure of the Si(110) surface, and a widely accepted model has not been proposed. In the earlier LEED study, Sakurai and Hagstrum (1976) showed that the original 5×1 structure for the clean surface disappeared during hydrogen exposure and was replaced by a 1×1 LEED pattern. They suggested that the 5×1 reconstruction was due to the relaxation of surface Si atoms rather than due to surface vacancies, though no specific structure model was proposed. Angle-resolved ultraviolet photoelectron spectroscopy (ARUPS) work (Mårtensson *et al.* 1985) reported that π-bonded chains were an essential part of the reconstructed Si(110) 5×1 surface. Recent STM work by Becker *et al.* (1988) showed the absence of the two first layer chains (tubes) per surface unit cell. The missing chains were oriented along the $[\bar{1}10]$ direction. In the missing chains they observed terrace structures, which were found to consist of two tetramers per unit cell. The individual protrusions of the tetramers were suggested to be 1·0 Å above the (110) tubes of the substrate and were related to adatoms based on the STM image. The unit cell was measured to be approximately 27·5×16 Å. Neddermeyer and Tosch (1988) have observed with a STM a 2×5 periodicity of atomic building blocks which corresponds to a 4×5 LEED pattern. These building blocks were arranged in the form of chains along the $[\bar{1}10]$ directions. They could distinguish two types of adatoms and argued that 18 out of 20 dangling bonds are saturated by 6 adatoms, leaving two dangling bonds per unit cell unsaturated. They also observed some distortions at least in the top two layers compared with the ideal surface. In more recent work using spectroscopic differential reflectometry (SDR), AES and LEED by Keim *et al.* (1990), it was shown that the prominent 5×1 structure is streaked with diffuse spots along the $[\bar{1}10]$ direction, but could be reconciled by a mixture of 5×1, 5×4 and 5×5 higher order structures.

Fig. 1*a* shows the unreconstructed Si(110) surface. The surface layer contains chains of Si atoms having two bonds along the chain and one bond towards the second layer chain. Similar to the Si(111) surface, Si(110) is characterised by one dangling bond per surface atom. Different structural models for the Si(110) 5×1 surface have been mentioned or proposed in both theoretical and experimental studies. These models can be classified as follows: a missing row or simple vacancy model mentioned by Olshanetsky and Shklyaev (1977), a terrace or step model suggested by Nesterenko *et al.* (1988), and an adatom model proposed by Keim *et al.* (1990). The schematic representations of these models are shown in Figs 1*b–d* respectively. In all unit cells proposed the second and third layers are considered to have their ideal bulk structure. The missing row model in Fig. 1*b* involves six vacancies (or 40% vacancy sites) in the 5×1 unit cell. The terrace model in Fig. 1*c* is characterised by two individual terraces, each of which is separated by double lattice spacing, and is assumed to be 1·92 Å [a bulk Si(110) lattice spacing] above the outermost layer. The complicated adatom model (Fig. 1*d*) is based on a reduction of dangling bonds which is due to the formation of adatoms. It consists of the coexistence of adatoms, nonadatoms and rest atoms and various reconstructions (Keim *et al.* 1990).

In the present study, attempts have been made to solve this complex issue by studying a clean Si(110) 5×1 surface with the technique of low energy ion

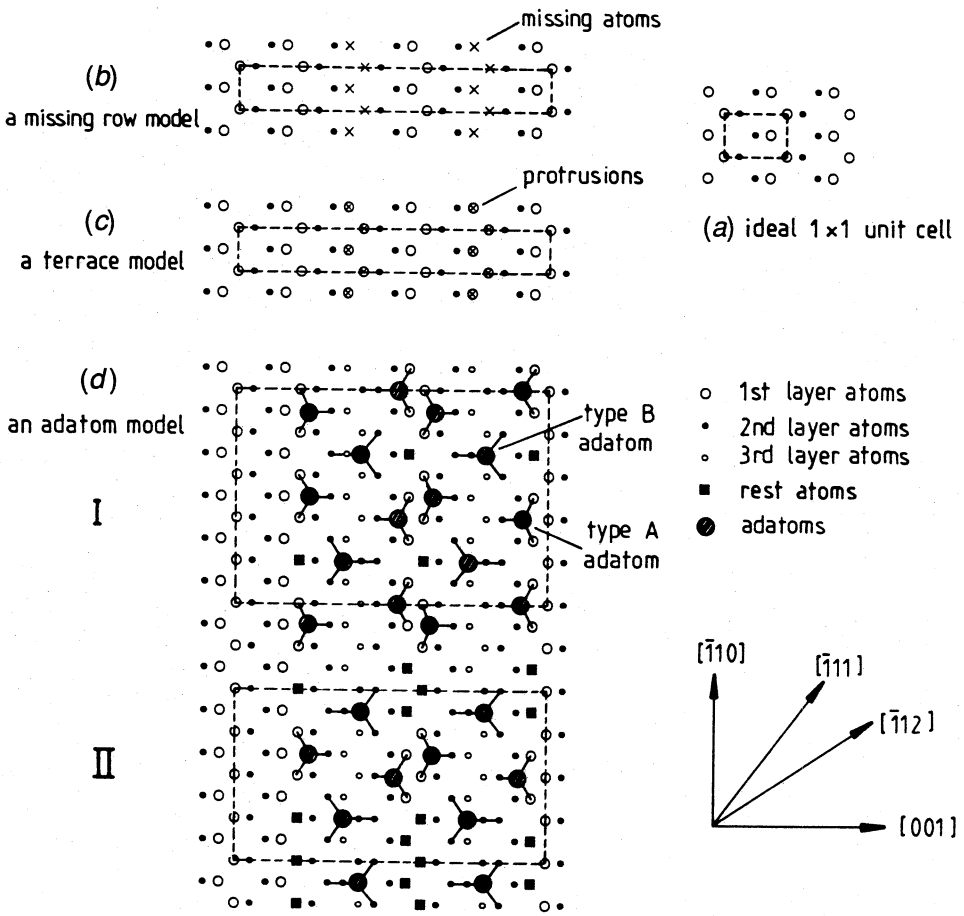

Fig. 1. The ideal Si(110) and proposed models of the Si(110) 5×1 surfaces: (*a*) the 1×1 unit cell; (*b*) a missing row or simple vacancy model; (*c*) a terrace model with protrusions the height of a bulk layer spacing 1·92 Å; and (*d*) an adatom model proposed by Keim *et al.* (1990) which shows a schematic representation of the reconstructed Si(110) surface with various reconstructed models for the unit cell considered.

scattering (LEIS) which has the advantage of obtaining information concerning the atomic arrangement of the surface layers, realising that the Si(110) 5×1 surface may have a different structure to that of the models proposed. This structure is measured from scattered spectra as a function of incident angle α and azimuthal angle ϕ at a constant scattering angle. The experimentally obtained backscattered angular distributions were then compared with computer simulations of the scattering process based on various structural models of the surface described above. The use of noble gas projectiles, which have an extremely high rate of neutralisation during scattering events, ensures a high degree of

surface sensitivity (see e.g. Aono 1984). It also reveals some characteristics of the relationship between the top layer and layers below, something that is difficult for STM to achieve. Although detailed quantitative interpretation of the full range of ion scattering data from the Si(110) 5×1 structure is difficult to achieve, there is clear evidence for a major reconstruction of the surface. Moreover, a reasonable fit for the adatom model between the experimental data and computer simulation shows that the clean Si(110) 5×1 surface consists of a real coexistence of several different phases with partial disorder along the $[\bar{1}10]$ direction.

2. Experimental

Our experimental apparatus has been described previously (O'Connor *et al.* 1988; Shen *et al.* 1992). In brief, the LEIS experiments using 2 keV He^+ ions were conducted in system A and a LEED pattern check of the clean Si(110) surface was performed in system B. System A was a Leybold–Heraeus three-dimensional angular resolved energy spectrometer operating in the constant retardation mode with an energy resolution ($E/\Delta E$) of 200. This system was fitted with a 3M minibeam ion gun. A spherical electrostatic analyser (ESA) could be rotated about the sample allowing variation of the total laboratory scattering angle θ from 0 to 135°. Later it was possible to transfer the target to system B equipped with rear view LEED optics. Both vacuum chambers were pumped by a combination of turbomolecular and titanium sublimation pumps which achieved a base pressure less than 10^{-10} mb in system A, while in system B it was typically 2×10^{-10} mb. The typical beam current density in system A was estimated to be 5×10^{-8} A cm^{-2}. Si peak signals were measured in 6 s, which corresponds to 2×10^{12} ions cm^{-2} of ion dose per measuring point. No significant surface damage was observed during the measurements. The incidence angle α and azimuthal angle ϕ were under computer controlled stepper motors to give a setting accuracy of 0·1°. The accuracies of the angles α, ϕ and θ were ±0·5°, ±1° and ±1° respectively. The incident angle scans were performed at fixed azimuth, i.e. [001], $[\bar{1}10]$ and $[\bar{1}12]$, by varying the angle between the beam and the surface from 0° (i.e. beam parallel to the target surface) to 50° in 1° intervals under stepper motor control. The target was annealed after each scan in order to avoid contamination and surface damage.

A mirror-polished p-type Si(110) single crystal ($10\times14\times0{\cdot}4$ mm^3) was used in this study. The resistivity of the target was 10 Ω cm. The target was cleaned in a CP4 etchant and then rinsed with distilled water prior to insertion into the vacuum chamber. No chemical etch was performed to remove the native oxide layer on the target. The Si(110) was mounted in a tungsten frame and heated radiantly to 500°C by a tungsten filament placed directly behind the target. Heating above 500°C was accomplished using electron bombardment. The temperature of the target was monitored with a thermocouple clamped to its side and by using an optical pyrometer. The target was cleaned using cycles of ion bombardment followed by high temperature annealing. Afterwards, a contamination check of the surface was made by He^+ scattering. Cleanliness was verified by the absence of C, O, S and Ni in the LEIS spectra (specifically less than 1% for C, S, Ni and other contaminants, and less than 0·1% for O). All measurements were made after annealing to 900°C and cooling to room

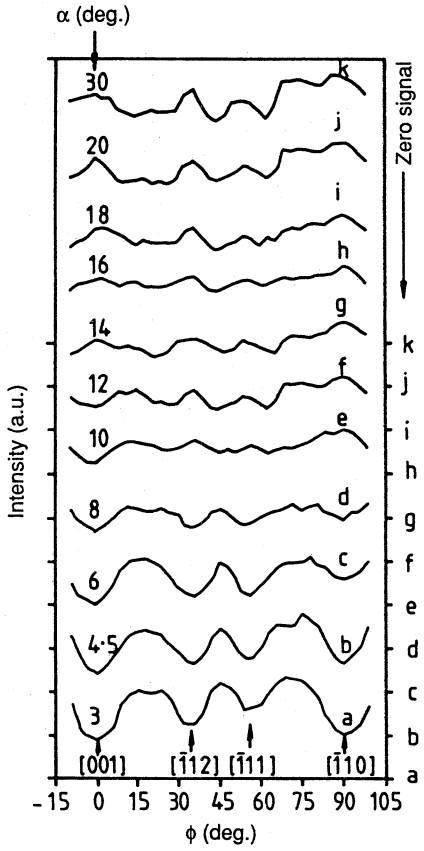

Fig. 2. Intensity of 2 keV He^+ ions scattered from the Si(110) 5×1 surface at the fixed scattering angle $\theta = 135°$ as a function of ϕ at various values of α, where α and ϕ are the incident and azimuthal angles respectively (α is measured from the surface).

temperature. LEED patterns of the clean Si(110) surface observed showed a 5×1 superstructure with diffuse spots and streaks along the $[\bar{1}10]$ azimuth. It was very difficult to obtain a sharp LEED pattern with low background. This pattern may represent a mixture of coexisting higher order structure and partial disorder along the $[\bar{1}10]$ azimuth. To examine whether or not other surface structures were formed by different heat treatment, long anneals (60 min) in the temperature range 300–900°C (temperature elevated stepwise every 100°C) were performed. However, the 16×2, 4×5, 2×1, 7×1, and 9×1 structures reported by Jona (1965) and Olshanetsky and Shklyaev (1977) were not observed.

3. Results

Scans of He^+ ions scattered from the Si(110) 5×1 surface were obtained as a function of the azimuthal angle ϕ and the incident angle α at a fixed scattering angle θ. The angle α is measured from the surface. Figs 2 and 3 show the ϕ and α dependences of the integrated peak area respectively. The neutralisation effect of the noble gas ions and the large scattering cross section at lower energies guarantees that the structural signals mainly come from the top two layers of the surface. The intensity reductions observed in Fig. 2 are due to shadowing effects, which should directly reflect the structure of the Si(110) 5×1 reconstructed surface. The most important feature in Fig. 3 (solid dots) is that there is only one

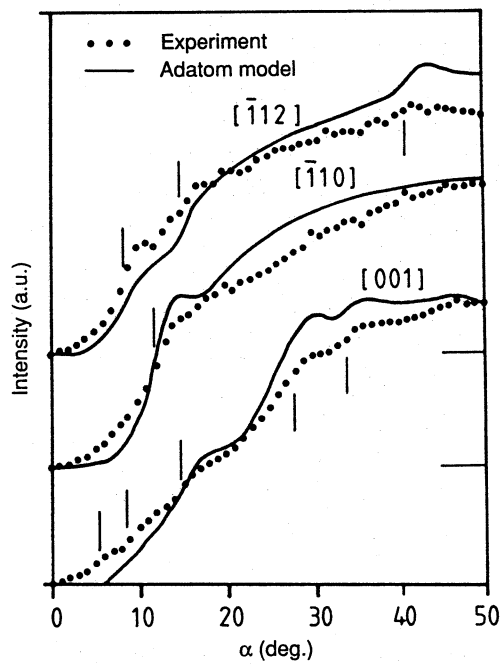

ϕ	A (×10^{15} s^{-1})	a (Å^{-1})	v_c (×10^5 m s^{-1})
[001]	3·0	1·0	2·7
[$\bar{1}$12]	2·4	1·2	1·7
[$\bar{1}$10]	3·5	1·8	1·6

Fig. 3. Experimentally measured intensity (solid dots) of 2 keV He^+ ions scattered from the Si(110) 5×1 surface at the fixed scattering angle $\theta = 135°$ as a function of α along three different azimuthal directions. The solid vertical lines indicate the position of the shadowing edges. The calculated intensities are shown by solid curves for the adatom model for comparison. The neutralisation model of Hagstrum is uswed in the calculation. The values used for the two parameters A and a (also v_c) are tabulated (for detail see Section 4).

α_c clearly visible for the [$\bar{1}$10] azimuth and there are two critical values of $\alpha_c = 8°$ and 15° along the [$\bar{1}$12] azimuth, while another shadowing edge at $\alpha = 41°$ along the [$\bar{1}$12] azimuth is too weak to be resolved individually. Along the [001] azimuth, there are a few shadowing edges. The critical angle is determined by both the shape of the shadow cone and the atomic arrangement of the surface atoms. By using the shape of the shadow cone determined from the Thomas–Fermi–Molière (TFM) potential for He^+–Si (see Fig. 4), a simple calculation can be made to obtain the critical angles expected for various structural models.

4. Computer Simulation, Quantitative Analysis and Discussion

To search for a suitable model which satisfies various structural features deduced from Figs 2 and 3, computer simulations have been performed as a

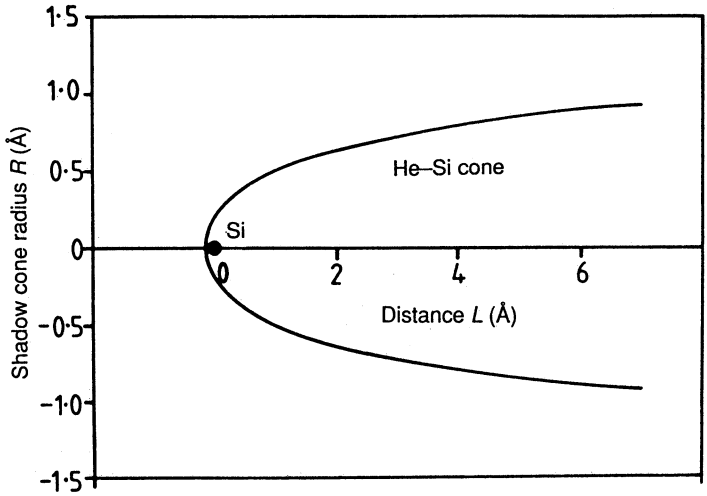

Fig. 4. Calculated shape of the shadow cone using the TFM potential with the screening length correction factor of $c(2,14) = 0{\cdot}77$ for 2 keV He^+ scattered from Si.

function of the incident angle to compare with experimental data. The intensities of scattered He^+ ions for various structural models of the Si(110) surface, i.e. the unreconstructed 1×1, the missing row, the terrace, and the adatom models, have been calculated for different low index azimuthal directions as a function of the incident angle α. Both shadowing and blocking effects were considered. The calculation was performed using the TFM potential, which is known to be suitable for describing the ion–atom interaction potential in the keV energy range if the screening length is chosen properly. The screening length correction factor c was determined with no free parameter from the empirical formula (O'Connor and Biersack 1986) $c(Z_1, Z_2) = 0{\cdot}045(Z_1^{1/2} + Z_2^{1/2}) + 0{\cdot}54$, where Z_1 is the atomic number of the primary particle and Z_2 is that of the target atom. For the combination of He and Si, we get $c(2,14) = 0{\cdot}77$.

In computer simulations the main aim of the method was to calculate the hitting probabilities where the deflection angle as a function of impact parameter is calculated, as discussed by Tromp and van der Veen (1983). The probability is sensitive to the relative thermal vibrational amplitude of the atoms in the crystal. The total scattered intensity was regarded as the sum of encounters with an array of two atoms and was calculated for each atom group by determining the probability density that an incident ion could hit a target atom along a particular trajectory (see e.g. Sato *et al.* 1985; Porter *et al.* 1987, 1988; Huang and Williams 1988). The results of the individual calculations were then combined to simulate the desired crystal structure and scattering geometry. Because of the extremely high neutralisation rate for low energy noble gas ions, only the top two atom layers were considered in the simulation. The effective contribution from the second layer atoms was taken into account by assuming that the contribution decreases exponentially with increasing distance from the first layer (Englert *et al.* 1982). A root-mean-square displacement $\langle u^2 \rangle^{1/2}$ of $\rho = 0{\cdot}15$ Å was chosen for the thermal vibration amplitude of surface Si atoms. Fig. 5 shows the calculated angular scan for three values of the rms displacement, indicating substantial

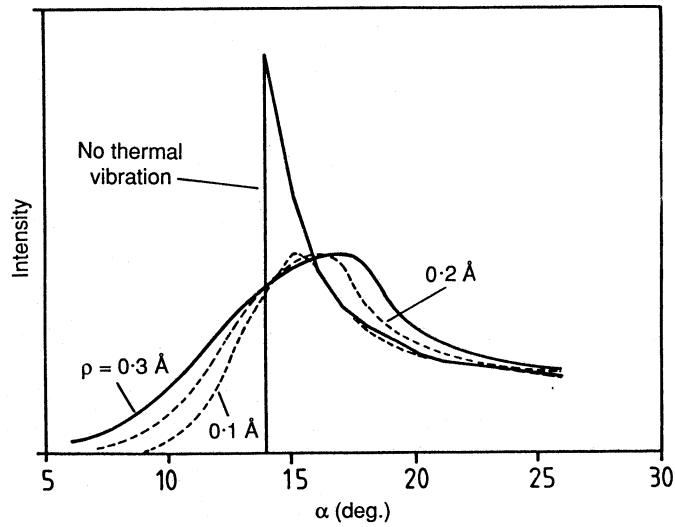

Fig. 5. Computer simulation of a 2 keV He^+ beam intensity as scattered by Si atoms as a function of the incident angle for the nonvibrating and the vibrating lattice. The three curves for the vibrating lattice have been normalised to each other.

weakening of the focusing effect due to surface atom vibrations. Neutralisation effects were taken into account using the Hagstrum (1954) model. The values of two parameters, A and a, have been chosen to fit the experimental data with each model, resulting in different characteristic velocities $v_c = (A/a)\exp(-ar_0)$ along the different azimuths. In the experiment performed here, the distance of closest approach r_0 (using the Molière approximation to the Thomas–Fermi potential) is calculated to be 0·12 Å for 2 keV He^+ at $\theta = 135°$. The larger the value of A, the faster the rate of neutralisation, while a large value of a reflects a more localised electron transfer region surrounding the individual Si atoms. However, these values of A and a were found in this study not to be unique, since a range of combinations produced almost equal simulation results. Figs 6 and 3 (solid curves) show all the calculated intensities of scattered He^+ ions as a function of α along the different azimuths using the Hagstrum neutralisation model. The values of A and a for three azimuth angles which fitted the experimental data are tabulated in each figure. It is evident that the calculated intensity along the $[\bar{1}10]$ direction is identical for the 1×1 model, the missing row model and the terrace model, since the Si atom arrangements along this direction for these three cases are the same.

For the ideal surface (Fig. 6*a*), the scattering intensity starts to rise only when α is larger than the critical angle α_c. This is due to the fact that the shadow cones are so wide that all surface atoms are shadowed from the incoming ion beam by their neighbour atoms at small incident angles. With increasing incidence angle, the surface atoms begin to move out of the shadow cone at the critical angle α_c which results in a sudden increase of scattered ions. For example, the intensity for the $[\bar{1}10]$ azimuth in Fig. 6*a* drops to zero for $\alpha < 10°$. This is due to every first layer Si atom being shadowed by its adjacent first layer atom, and every

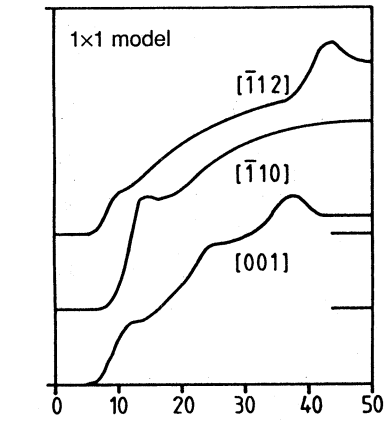

(*a*)

ϕ	A (×10^{15} s^{-1})	a (Å^{-1})	v_c (×10^5 m s^{-1})
[001]	4·2	1·5	2·3
[1̄12]	2·5	1·8	1·1
[1̄10]	3·5	1·85	1·5

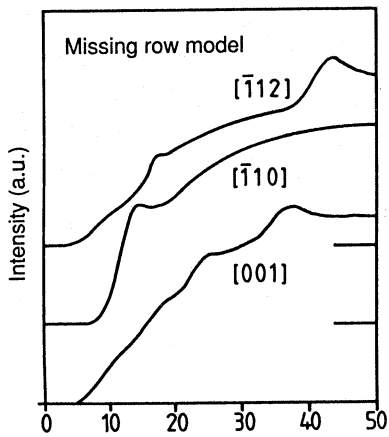

(*b*)

ϕ	A (×10^{15} s^{-1})	a (Å^{-1})	v_c (×10^5 m s^{-1})
[001]	2·8	1·2	2·0
[1̄12]	3·2	1·6	1·7
[1̄10]	3·5	1·85	1·5

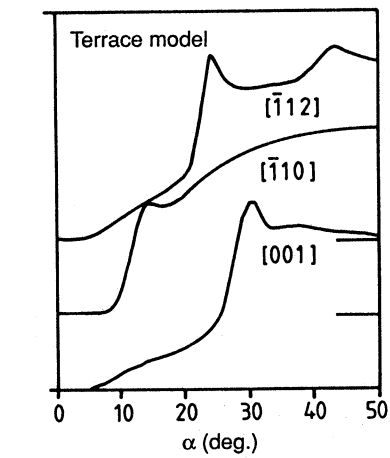

(*c*)

ϕ	A (×10^{15} s^{-1})	a (Å^{-1})	v_c (×10^5 m s^{-1})
[001]	2·5	1·5	1·4
[1̄12]	3·0	1·2	2·2
[1̄10]	3·5	1·85	1·5

Fig. 6. Calculated intensities of 2 keV He^+ ions scattered from the Si(110) surface at $\theta = 135°$ as a function of the incident angle α for (*a*) the unreconstructed 1×1 model; (*b*) the missing row model; and (*c*) the terrace model. The results for azimuths [001], [1̄10] and [1̄12] are shown. The neutralisation model of Hagstrum (1954) was used in the calculation. The values used for the two parameters A and a (also v_c) are tabulated.

second layer Si by its adjacent second layer atom. The adjacent Si–Si spacing is 3·84 Å. The [$\bar{1}$12] azimuth has a shadowing edge at $\alpha = 8°$ and drops to zero at $\alpha \leq 5°$. The intensity along the [001] azimuth has a sharp shadowing edge at $\alpha = 9°$ and drops to zero for $\alpha \leq 6°$. The other edges observed in these curves at large α values are the shadowing effects between the first and second layer atoms. In contrast to this, the experimental incident angle scan results in Fig. 3 (solid dots) exhibit weak shadowing edges along all the azimuthal directions compared with that for the calculation. Furthermore, structures calculated at $\alpha \approx 23°$ and 35° in the azimuth [001] in Fig. 6*a* were not observed experimentally (Fig. 3) and the shadowing edge at $\alpha = 41°$ along the [$\bar{1}$12] azimuth is too weak.

Analysis also shows that the intensity distributions for both the missing row model in Fig. 6*b* and the terrace model in Fig. 6*c* are unacceptable. The main differences between the missing row model (Fig. 6*b*) and experimental data (Fig. 3) are: the shadowing edge at $\alpha = 8°$ along the [$\bar{1}$12] azimuth is too weak in Fig. 6*b*, and the structure at $\alpha = 28°$ along the [001] azimuth observed in Fig. 3 does not appear in Fig. 6*b*. Other possibilities for the missing row model (for example, four vacancies per unit cell, i.e. 26·7% vacancy sites) have also been tested. Analysis indicates that they are unacceptable. The terrace model calculated in Fig. 6*c* also cannot explain all of the observed intensity variations in the [$\bar{1}$12] and [001] azimuths. It is obvious that the experimental results do not agree with either the missing row or the terrace model.

From these observations it can be concluded that the 5×1 structure is caused by a more drastic reconstruction, possibly by coexistence of a few different structures. The weak shadowing edges at lower α values along both [001] and [$\bar{1}$10] are indicative of the presence of additional scattering centres. In this sense the adatom model proposed recently by Keim *et al.* (1990) warrants attention. This model is represented by the various reconstructions based on an adatom-like higher order structure. In the absence of a credible, widely accepted model of the 5×1 surface, and in view of its complex nature, comprehensive LEIS experiments need to be conducted along numerous azimuths on the surface in order to arrive at a detailed model. Nevertheless, preliminary LEIS angular scans are presented here which may help to identify the possible reconstructed model. For simplicity, a combination of the adatom model I (5×5 atructure) and model II (5×4 structure) with the same fraction is assumed. Although the 5×3 structure will result in a maximum reduction of dangling bonds from 24 to 8 (Keim *et al.* 1990), it is excluded because the adatoms seen in a STM study (Neddermeyer and Tosch 1988) are located at rather asymmetric positions. Also, this 5×3 structure has never been reported by LEED. To differentiate the atomic arrangement between the theory and experiment, particular attention is paid to major results along the [001] azimuth. Referring to Fig. 1*d*, if the He^+ ions are directed along the [001] azimuth, surface adatoms and vacancies are symmetrically aligned with about twice the normal lattice constant of 5·43 Å. It is most likely that the adatoms will shadow the rest atoms, and the Si atoms in the first and second layers depending on the height of the adatoms. In the simulations it is assumed that the adatoms have the same dangling bond length, i.e. they occupy the symmetrical sites corresponding to two first layer atoms and one second layer atom (type-A adatom), as well as three second layer atoms (type-B adatom), as shown in Fig. 1*d*. To achieve the best fit with the adatom model, the type-A and type-B adatoms were found to sit symmetrically 1·0±0·3 Å above the first

layer Si atoms and 1·9±0·2 Å above the second layer respectively, and the rest atoms are located at the ideal top layer positions. Comparison of the calculated results with the experimental data was quite satisfactory.

As can be seen, the adatom model is in fair agreement with the experimental results (Fig. 3). For example, a very faint shadowing edge at $\alpha = 6°$ observed along [001] is due to the combined effects of adatom shadowing adatom and Si shadowing Si in the first layer. Such scattering centres create a strong surface roughness locally, where shadowing is weakened and focusing collisions from one side of the adatom site onto adatoms on the other side (also from one side of the vacancy site onto atoms on the other side) are likely to occur. The other shadowing edges observed occur at $\alpha = 9°$ for the first layer Si shadowing; at $\alpha = 15°$ for the adatom shadowing the first layer Si; at $\alpha = 28°$ for the adatom shadowing the second layer Si; and at $\alpha = 33°$ for the first layer Si shadowing the second layer Si. Other shadowing edges are not resolved individually due to combined shadowing and blocking effects of the adatoms, rest atoms and Si atoms in the top two layers encountered at higher incident angle. Along the $[\bar{1}10]$ azimuth, only one major experimental shadowing edge is observed and it occurs at 12°, which is expected for both the first layer Si and second layer Si shadowing. Notably, there is some scattering intensity below 10°, which is ascribed to the partial disorder effect and asymmetrical adatom spacing along the $[\bar{1}10]$ azimuth. Along $[\bar{1}12]$ there are two critical angles $\alpha_c = 8°$ and 15° visible, corresponding to the first layer Si shadowing first layer Si and first layer Si shadowing second layer Si (second nearest neighbour) respectively. Another critical angle $\alpha_c = 41°$, due to first layer Si shadowing second layer Si (nearest neighbour), predicted for the $[\bar{1}12]$ azimuth was too weak to be resolved in the experimental scan. The reason for this is not clear, though overlapped shadowing and blocking effects and multiple scattering in the top few layers might be responsible. The model is also consistent with the experimental results shown in Fig. 2. For example, the sharp decreases in intensity observed for α below 8° along [001], $[\bar{1}10]$ and $[\bar{1}12]$ are due to shadowing effects. The increase observed along $[\bar{1}10]$ and $[\bar{1}12]$ at $\alpha = 10°$ is due to focusing effects. The fact that the intensities below the critical angles in the experimental scans were clearly observed is attributed to surface defect or disorder effects. It seems to be consistent with the LEED observation, i.e. it shows streaks and diffuse spots with a high background. A determination of the exact structural parameter of the reconstruction model is clearly difficult, but it is strongly suggested from the present LEIS results that there is evidence of higher order reconstruction and some disorder along the $[\bar{1}10]$ azimuth. Although the experimental data appear to support the adatom model (a combination of model I and II) derived by Keim *et al.* (1990) based on the STM images (Becker *et al.* 1988; Neddermeyer and Tosch 1988), such a conclusion is not unequivocal. For example, the first two layer Si atoms are assumed to be at the ideal positions except that there are two missing chains along the $[\bar{1}10]$ azimuth. The STM images (Neddermeyer and Tosch 1988), however, show that at least the second atomic layer is severely distorted compared with the ideal structure. Also, the height of adatoms and rest atoms is not sensitive to the simulated incident angle scan because of the complicated higher order 5×1 structure.

Two kinds of adatom height have been proposed in the simulation, for the adatom model which corresponds to two different values of dangling bonds, i.e. 3·0 Å for type-A adatom and 3·14 Å for type-B adatom. The UPS study by

Martensson *et al.* (1985) showed several similarities between the Si(110) 5×1 surface and the cleaved Si(111) 2×1 surface. The topmost planes in Pandey's (1981) model of the Si(111) 2×1 surface have a chain-like structure which resembles the atomic configuration of the ideal Si(110) surface. An interesting result from their study was that the surface state feature observed at ~0·8 eV below the Fermi level E_F on Si(110) 5×1 was found to exhibit dangling bond character, and was broader than that on Si(111) 2×1. This might be attributed to disorder effects of the Si(110) 5×1 surface. STM measurements by Becker *et al.* (1988) showed an occupied state at ≈1 eV (in agreement with the filled state found by UPS) which is associated with the direction between the adatom containing atom B and the unoccupied states at about 1 and 2 eV which are related to adatoms. Keim *et al.* (1987) determined that this surface has empty states at about 0·9 and 1·7 eV above the Fermi level. The occupied states at ~0·8 and 2·4 eV below E_F could be identified with the rest atom and *A*-type atoms respectively. Other structures of Si(110) formed by different heat treatment such as 7×1, 9×1 and 2×1 are thought to be caused by the potential distortion with varying dimensions along the [001] direction.

5. Discussions

A survey of the literature has revealed no detailed calculation of the atomic and electronic structure of the reconstructed Si(110) surface. A large number of superstructures observed from the Si(110) surface are not yet understood. In the present study an attempt has been made to probe the atomic arrangement of the Si(110) 5×1 surface which was observed by LEED.

For the adatom and rest atom sites suggested here, reasonable agreement between computer simulation and experimental data occurs with the type-A adatom placed 1·0±0·3 Å above the first layer Si plane, the type-B adatom placed 1·9±0·2 Å above the second layer Si plane and the rest atom placed in the ideal surface Si atom position. This does not conflict with the STM results by Neddermeyer and Tosch (1988), who observed two kinds of protrusions with differing heights at positive target bias (1 and 2 V) in V-shaped contours. There is no other experimental evidence at this time to support the adatom or rest atom height. A reliable measurement of the spacing between the adatom rows will provide the answer, though STM is unable to distinguish this. This will require LEIS experiments along a variety of azimuths in addition to [001], [$\bar{1}$10] and [$\bar{1}$12]. Experimental evidence suggests a definite coexistence of several higher order structures with partial disorder, which makes it the most complicated low index Si crystal to study.

Further experiments with LEIS using time-of-flight detection combined with 3D computer simulation may be necessary for a complete determination of this interesting surface. Also, detailed LEED I–V analysis combined with STM studies is required to confirm or refute the details of this adatom model for the higher order structure.

Acknowledgments

The authors gratefully acknowledge the financial support of this work by the Australian Research Grants Scheme.

References

Aono, M. (1984). *Nucl. Instrum. Methods* B **2**, 374.
Becker, R. S., Swartzentruber, B. S., and Vickers, J. S. (1988). *J. Vac. Sci. Technol.* A **6**, 472.
Englert, W., Taglauer, E., and Heiland, W. (1982). *Surf. Sci.* **117**, 124.
Hagstrum, H. D. (1954). *Phys. Rev.* **94**, 336.
Huang, J. H., and Williams, R. S. (1988). *Phys. Rev.* B **38**, 4022.
Ichinokawa, T., Ampo, H., Miura, S., and Tamura, A. (1985). *Phys. Rev.* B **31**, 5183.
Jona, F. (1965). *IBM J. Res. Develop.* **9**, 275.
Keim, E. G., van Silfhout, A., and Woherbeek, L. (1987). *J. Vac. Sci. Technol.* A **5**, 1019.
Keim, E. G., Wormeester, H., and van Silfhout, A. (1990). *J. Vac. Sci. Technol.* A **8**, 2747.
Mårtensson, P., Hansson, G. V., and Chiaradia, P. (1985). *Phys. Rev.* B **31**, 2581.
Neddermeyer, H., and Tosch, St. (1988). *Phys. Rev.* B **38**, 5784.
Nesterenko, B. A., Brovii, A. V., Maznichenko, A. F., and Kazakova, N. A. (1988). *In* 'Physics of Solid Surfaces' (Ed. J. Konkal), p. 101 (Elsevier: Amsterdam).
O'Connor, D. J., and Biersack, J. P. (1986). *Nucl. Instrum. Methods* B **15**, 295.
O'Connor, D. J., Shen, Y. G., Wilson, J. M., and MacDonald, R. J. (1988). *Surf. Sci.* **197**, 277.
Olshanetsky, B. Z., Repinsky, S. M., and Shklyaev, A. A. (1977). *Surf. Sci.* **64**, 224.
Olshanetsky, B. Z., and Shklyaev, A. A. (1977). *Surf. Sci.* **67**, 581.
Pandey, K. C. (1981). *Phys. Rev. Lett.* **47**, 1913.
Porter, T. L., Chang, C. S., Knipping, U., and Tsong, I. S. T. (1987). *Phys. Rev.* B **36**, 9150.
Porter, T. L., Chang, C. S., and Tsong, I. S. T. (1988). *Phys. Rev. Lett.* **60**, 1739.
Sakurai, T., and Hagstrum, H. D. (1976). *J. Vac. Sci. Technol.* **13**, 807.
Sato, K., Kono, S., Tenuyama, T., Higashiyama, K., and Sagawa, T. (1985). *Surf. Sci.* **158**, 644.
Shen, Y. G., O'Connor, D. J., and MacDonald, R. J. (1992). *Surf. Sci.* (in press).
Tromp, R. M., and van der Veen, J. F. (1983). *Surf. Sci.* **133**, 159.
Yamamoto, Y., Ino, S., and Ichikawa, T. (1986). *Japan. J. Appl. Phys.* **25**, L331.

Manuscript received 20 June, accepted 15 November 1991